Int. J. Electrochem. Sci., 17 **(2022)** Article Number: 220233, doi: 10.20964/2022.02.28

International Journal of
ELECTROCHEMICAL
SCIENCE
www.electrochemsci.org

Preparation of Sn_3O_4 Modified Ti/Black TiO_2 Electrode with Enhanced Photoelectrocatalytic Performance for Water Remediation

Zeqi Jiang[†], *Jian Zhang*[†], *Wenfeng Li*, *Pengyuan Wang*[*], *Guowen Wang*, *Hongchao Ma and Yinghuan Fu*[*]

School of Light Industry & Chemical Engineering, Dalian Polytechnic University, No. 1 Qinggongyuan, Ganjingzi District, Dalian, 116034, People's Republic of China
[*]E-mail: wangpengyuan@dlpu.edu.cn, fuyinghuan@sina.com
[†]The first two authors contributed equally to this paper

Received: 2 November 2021 / *Accepted:* 10 December 2021 / *Published:* 5 January 2022

Bio-refractory wastewater from the dyeing and finishing process has become a critical environmental problem. Semiconductor photoelectrocatalytic (PEC) technology is one of the most effective methods to remove organic pollutants from effluents, while the performance of photoanodes can significantly affect degradation efficiency. Herein, novel heterostructure composite photoanodes were synthesized through assembling various amounts of Sn_3O_4 nanosheets on the hydrogenated TiO_2 sheets to degrade the Reactive Brilliant Blue KN-R (RBB KN-R) solution. The hydrogenation expanded the optical absorption range improving the utilization of sunlight. And the incorporation of Sn_3O_4 nanosheets increases the electrochemically active area, promotes interfacial carrier transport, enhances interfacial carrier transport and facilitates the generation of reactive radicals during PEC. The composite electrode (Sn_3O_4-Ti/b-TiO_2) showed excellent degradation performance over 85% degradation of (RBB KN-R within 120 min and quite stable in 5 degradation cycles, holding great promise in accelerated degradation of dyeing wastewater.

Keywords: Heterostructure, Water remediation, Photoelectrocatalysis, Sn_3O_4,

1. INTRODUCTION

Dye wastewater with intense color, complex organic composition and limited biodegradability has been a challenging problem in industrial wastewater treatment and has attracted widespread attention[1,2,3,4]. A variety of methods such as Chemical coagulation [6], adsorption[5], biological oxidation[7], electrochemical oxidation[8] and photocatalytic[9] have been applied for its treating. However, these conventional methods are unable to treat the effluents effectively and thoroughly

[10,11,12]. Semiconductor photoelectrocatalytic (PEC) methods possess synergistic effects of electrocatalysis and photocatalysis are providing effective decolorization of dye-containing effluents [13]. PEC degradation technology of dyes is initiated by the activation of a semiconductor photoanode *via* illumination, then the photogenerated electron/hole pairs are separated under the assistance of electric fields, and active free radicals are generated in the solution to oxidize and degrade the dye molecules[14,15,16]. Therefore, the optical and electrocatalytic properties of the photoanode materials are the key influencing factors of the PEC process[17,18]. Massive efforts have been made to develop varies of semiconductor photoanode materials, including RuO_2 [19,20], IrO_2 [21], PbO_2 [22], TiO_2 [23], SnO_2 [24], and boron-doped diamond (BDD) anodes[25].

TiO_2 is a common material employed in photocatalytic (PC)/electrocatalytic (EC) processes for the oxidative disposal of organic pollutants[26]. With the advantages of a long lifetime of electron-hole pairs, compatible energy place of the conduction-valence band, excellent chemical-thermal stability and well catalytic property, it has attracted remarkable attention in recent years[27, 28]. In 1972, Fujishima and Honda introduced the application of n-type TiO_2 electrodes for electrochemical photolysis of water to PEC technology[29]. Later, Vinodgopal et al. used granular TiO_2 film electrodes in 1996 to degrade organic pollutants during the PEC process[30]. Nevertheless, Lower utilization of sunlight and fast electron-hole pair recombination lead to the low quantum efficiency of TiO_2, which impedes its application in PEC procedures[31, 32]. To overcome the shortcomings above, Chen et al. treated TiO_2 nanocrystals by hydrogenation and synthesized black TiO_2 extending its optical absorption to the infrared region (~1150 nm) in 2011[33]. Hydrogenation can cause structural and chemical defects in TiO_2 crystalline, resulting in long wavelength spectral absorption, which can improve the sunlight usage efficiency and enhance its electrical conductivity.[34] Besides, adding narrow band gap semiconductors (NiO[35], CuS[36], NiS[37], MoS_2[38], WO_3[39], Ag_2O[40] and Sn_3O_4[41]) as photosensitive components with TiO_2 to construct heterojunction structures provides fast transfer of photogenerated electrons and suppresses electron/hole pair recombination, which improves the quantum efficiency of TiO_2 electrodes[42]. Sn_3O_4 is an n-type semiconductor with a bandgap of 3 eV, that exhibits high room temperature resistance and a layered structure with the mixed valence of Sn^{2+} and Sn^{4+}, demonstrating outstanding PC activity in the degradation of organic pollutants and hydrogen production[43,44,45]. Consequently, the new heterostructured photoelectrodes constructed by coupling Sn_3O_4 and black TiO_2 will exhibit high PEC efficiency with the synergistic catalytic effect of the two materials.

In this study, we fabricated a novel photoelectrode combined with black TiO_2 and Sn_3O_4 nanosheets (Sn_3O_4-Ti/b-TiO_2) through a two-step hydrothermal process. A series of as-synthesized Sn_3O_4-Ti/b-TiO_2 composite photoelectrodes were analyzed *via* changing the concentration of the hydrothermal solution and detailed opto-electronic measurements were conducted for seeking the optimal preparation conditions. And the Sn_3O_4-Ti/b-TiO_2-3 is the most outstanding one demonstrating the degradation rate of 85 % and long-term stability for the degradation of Reactive Brilliant Blue KN-R (RBB KN-R) in 0.1 mol/L Na_2SO_4 solution. The possible mechanism of the PEC process was analyzed and explored by fluorescence quenching experiments. The photoelectrodes constructed with the black TiO_2 and Sn_3O_4 heterostructure hold great potential for practical applications in the decomposition of organic pollutants.

2. EXPERIMENTAL SECTIONS

2.1. Reagents and materials

Titanium sheets (99.7% pure) were purchased from Yunjiemetal Company. Oxalic acid ($C_2H_2O_4$), acetone ($C_4H_9N_3O$), benzoic acid, isopropanol (IPA), EDTA-2Na^+, L-ascorbic acid (LA), dilute hydrochloric acid (HCI), stannous chloride ($SnCl_2 \cdot 2H_2O$), trisodium citrate ($C_6H_5Na_3O_7$), sodium hydroxide (NaOH), sodium chloride (NaCl), sodium sulfate (Na_2SO_4), sodium dodecylsulfonate ($C_{12}H_{25}NaO_3S$) and reactive brilliant blue KN-R were purchased from Tianjin Chemical Reagent Company. All chemicals were of analytical grade and used as received. All solutions were prepared with deionized water.

2.2. Preparation of white TiO_2 electrode

Titanium sheet (70 mm×10 mm×1mm) was placed in a 10% oxalic acid aqueous solution and etched at 80°C for 2 h and then rinsed with deionized water. The etched titanium sheet was immersed in 5 M NaOH in an 80ml polytetrafluoroethylene (PTFE) lined stainless steel reactor for 6 h. After cooling down to room temperature, it was soaked in 1 M HCl and rinsing with deionized water. Then, the Ti sheets was dried at 60 °C in an oven and annealed in a muffle furnace at 450℃ with the heating rate of 2℃/min for 3 hours. The obtained sample was named Ti/w-TiO_2.

2.3. Preparation of black TiO_2 electrode

Putting Ti/w-TiO_2 into a tube furnace with hydrogen flow at 450°C for 7 hours, a black electrode was obtained and marked as Ti/b-TiO_2.

2.4. Preparation of Sn_3O_4-Ti/b-TiO_2 electrode

In a general process, 3 mmol $SnCl_2 \cdot 2H_2O$ and 7.5 mmol sodium citrate ($C_6H_5Na_3O_7$) were mixed with 50 ml deionization water thoroughly. 50mL 0.033 M NaOH solution was poured into an 80 mL PTFE lined stainless steel reactor with Ti/b-TiO_2 inside and heated at 180°C for 12 hours.

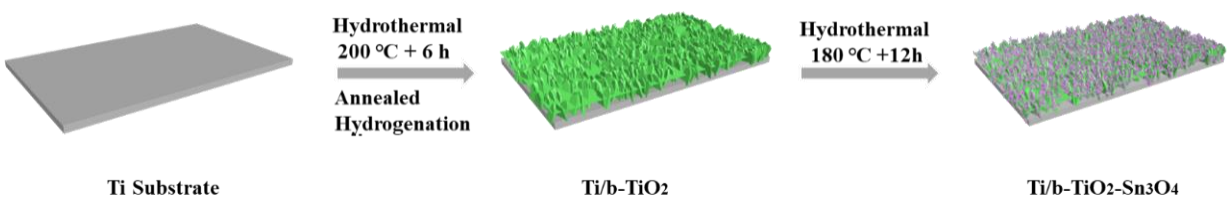

Scheme 1. Scheme for the preparation process of Sn_3O_4 modified hydrogenated TiO_2 electrode.

After cooling and washing with deionized water, the modified electrode was dried in a 60°C oven and labeled as Sn_3O_4-Ti/b-TiO_2-3. The Sn_3O_4-Ti/b-TiO_2-1, Sn_3O_4-Ti/b-TiO_2-2, Sn_3O_4-Ti/b-TiO_2-4 and Sn_3O_4-Ti/b-TiO_2-5 electrode were prepared with 0.011 M, 0.022 M, 0.044 M and 0.055 M NaOH solution sequently. The synthetic route of composite electrodes through the processes above were illustrated in Scheme 1.

2.5. Photoelectrocatalytic oxidation

The electrocatalytic performance of the electrode was evaluated by the decolorization efficiency of RBB KN-R solution with a concentration of 60 mg L^{-1} in a quartz reaction vessel. The cathode (Ti sheets) and anode (Ti/b-TiO_2-based eletrode) were parallel to each other and placed perpendicularly in the vessel with a distance of 30 mm. And 0.1 M Na_2SO_4 aqueous solution was used as the electrolyte. The simulated dye wastewater was prepared with 0.01g NaCl and 0.01g $C_{12}H_{25}NaO_3S$ added into the dye solution above. Electrocatalytic oxidation experiments was implemented with a direct current (DC) power supply at a continuous current density of 20 $mA \cdot cm^{-2}$. 10W ultraviolet lamp as the light source, the PEC oxidation was tested. Degraded aqueous solution were extracted from the reactor at certain intervals of time and then analyzed during the test. The removal rate (R_d) of RBB KN-R was calculated following the equation below:

$$R_d = (1 - A/A_0) \times 100\%$$

where A_0 and A stands for the initial and final absorbance of dye solution, respectively.

2.6. Characterizations

X-ray diffraction (XRD) was used to determine the composition of samples on a Shimadzu XRD 6100X diffractometer radiated by Cu Kα (λ = 1.5418 Å) with 40 kV in voltage, 30 mA in current. Scanning electron microscope (SEM, Hitachi-1510, Japan) equipped with an energy dispersive spectrum (EDS) system, transmission electron micrographs (TEM, JEOL JEM-2100) and high-resolution transmission electron microscopy (HRTEM, JEOL JEM-2100) were used for recording sample morphologies. X-ray photoelectron spectroscopy (XPS) was performed on a VG ESCALAB 250 electron spectrometer (Thermo VG) and use Al Kα monochromatic radiation as the X-ray source. The photoluminescence (PL) spectrum of the benzoic acid solution on each electrode was measured with a fluorescence spectrophotometer (Hitachi F-7000, Japan) under 440 nm excitation at 25nm. The electrochemical test collected on a CHI 660E potentiostat/constant current (Shanghai Chenhua Instrument Co., Ltd) with three-electrode standard system. A platinum plate and a saturated calomel electrode were used as counter electrode and reference electrode respectively.

3. RESULTS AND DISCUSSION

3.1. Synthesis and structural characteristics

The crystalline structures of as-synthesized electrodes were investigated by X-ray diffraction (XRD). Figure.1 present the XRD patterns of Ti/w-TiO_2, Ti/b-TiO_2 and Sn_3O_4 modified Ti/b-TiO_2 electrodes. The diffraction peaks of Ti/w-TiO_2 and Ti/b-TiO_2 electrodes could index well to TiO_2 (JCPDS 88–1175) and Ti substrates (JCPDS 44–1294). With Sn_3O_4 nanoparticles coating on the Ti/b-TiO_2 surface, the characteristic diffraction peaks of Sn_3O_4 (JCPDS 16-0737) appear. The morphologies of the prepared electrodes were monitored by scanning electron microscope (SEM) and shown in Figure. 2(a-g). Figure. 2(a-b) presented the surface image of Ti/w-TiO_2 and Ti/b-TiO_2 with fish-scale nanosheets grown. The hydrogenation reduction treatment did not affect the morphology and scale of the nanosheets. When Sn_3O_4 was introduced into the second step of the hydrothermal process, nanoparticles were gradually attached to the surface of the black TiO_2 flakes (Figure. 2 c-d). With the concentration of mother liquor increasing during the hydrothermal process, the nanoparticles expanded into nanoplates continuously (Figure. 2e). As the solubility of the mother liquor further increase, the Sn_3O_4 nanoplates will become enlarged and cover the Ti/b-TiO_2 completely (Figure. 2f-g). The energy dispersive spectrum (EDS) mapping images of Sn_3O_4-Ti/b-TiO_2-2 were collected in Figure. 2 (h-l), indicating the successful synthesis and uniform distribution of Sn_3O_4 nanoplates on the Ti/b-TiO_2 electrode surface.

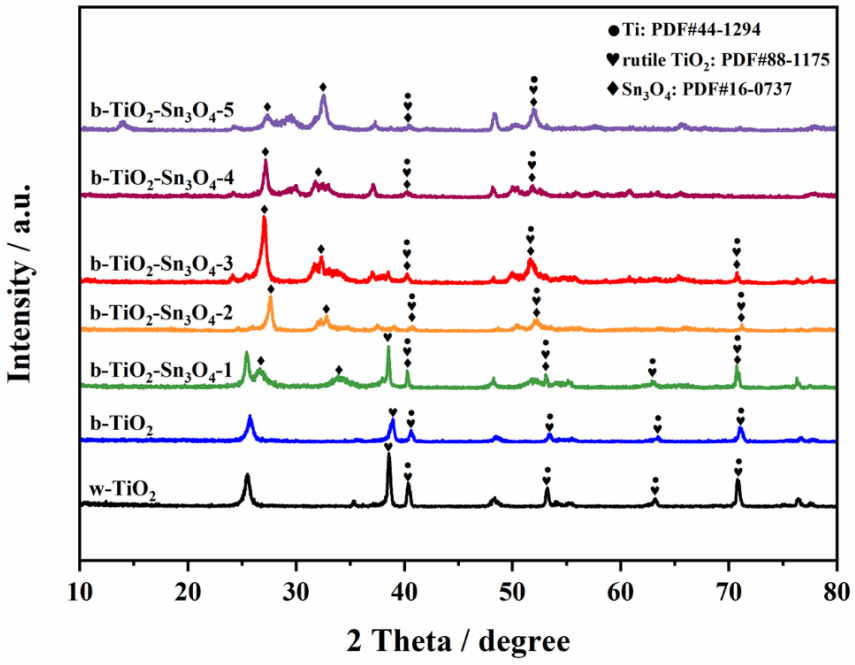

Figure 1 XRD patterns of Ti/w-TiO_2, Ti/b-TiO_2 and Sn_3O_4 modified Ti/b-TiO_2 electrodes.

For further study of the detailed internal morphology and structure in hybrid electrodes, transmission electron micrographs (TEM) tests were carried out and illustrated in Figure 3. Figure 3(a)

exhibited the Sn_3O_4-Ti/b-TiO_2-3 electrode with flower-like nanosheets and Sn_3O_4 nanoparticles attached. The adhered nanoparticles may increase the active area of the electrode and promote catalytic activity. And the compact bonding between Sn_3O_4 nanoparticles and TiO_2 nanosheets could promote the transfer of photogenerated charges to improve the charge separation efficiency. The high-resolution transmission electron microscopy images of the Sn_3O_4-Ti/b-TiO_2-3 electrode were presented in Figure 3(b-c). The lattice spacing of 0.216 nm and 0.329 nm could be observed in the heterostructure, corresponding to the (111) crystal plane in TiO_2 and Sn_3O_4, indicating that Sn_3O_4 uniformly adhered to the surface of black TiO_2 nanoflower.

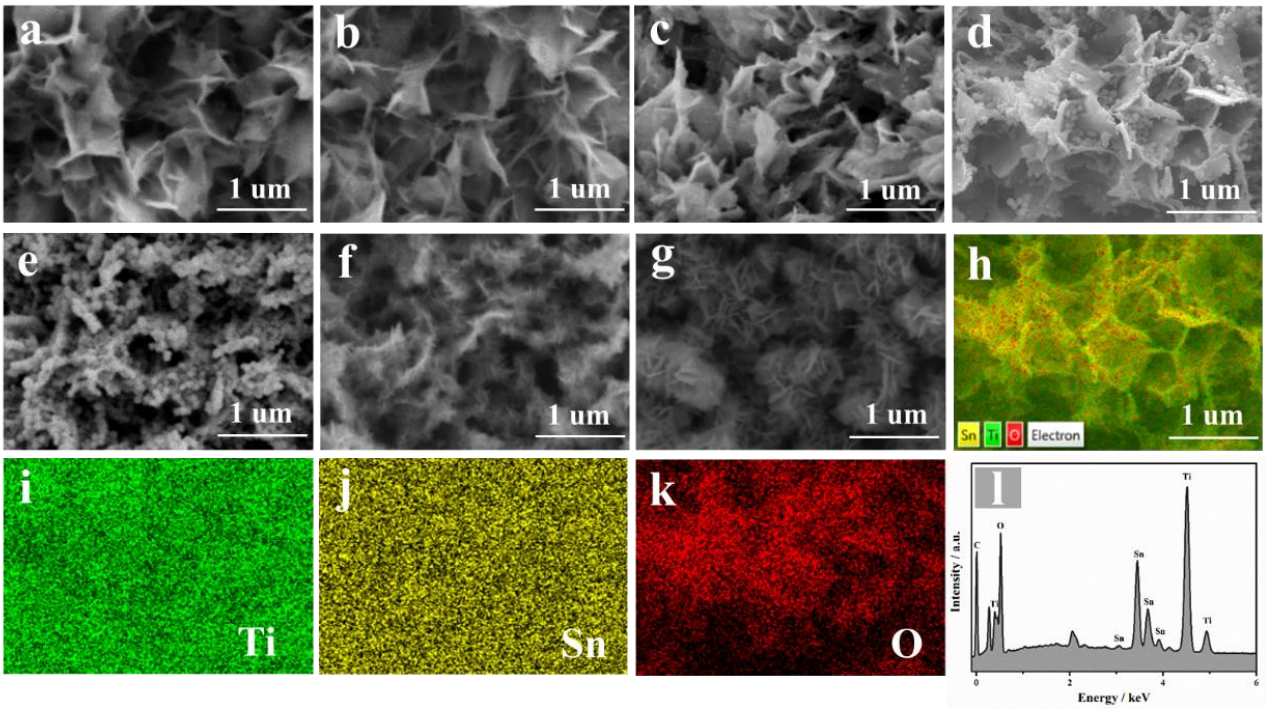

Figure 2. The SEM images of (a) Ti/w-TiO_2, (b) Ti/b-TiO_2, (c) Sn_3O_4-Ti/b-TiO_2-1, (d) Sn_3O_4-Ti/b-TiO_2-2, (e) Sn_3O_4-Ti/b-TiO_2-3, (f) Sn_3O_4-Ti/b-TiO_2-4 and (g) Sn_3O_4-Ti/b-TiO_2-5. (h-l) High-resolution SEM-EDS mapping analysis of Sn_3O_4-Ti/b-TiO_2-2.

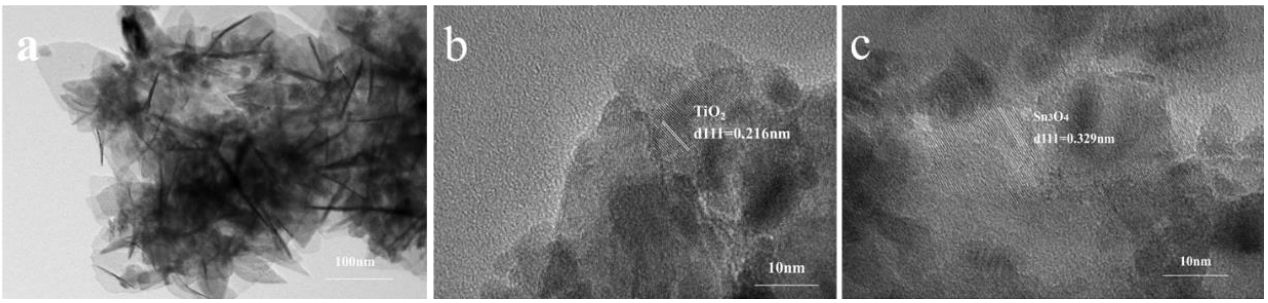

Figure 3. (a) TEM image of Sn_3O_4-Ti/b-TiO_2-3 electrode and (d) HRTEM image of Sn_3O_4-Ti/b-TiO_2-3 electrode.

X-ray photoelectron spectroscopy (XPS) was measured to analyze the chemical composition and valence state of Ti/b-TiO_2 and Sn_3O_4-Ti/b-TiO_2-3 electrodes and presented in Figure 4. Figure 4(a) exhibits the spectra of Ti/b-TiO_2 and Sn_3O_4-Ti/b-TiO_2 in a wide range of binding energy. In addition to the peaks of Ti 2p and O 1s, additional signal peaks of the element Sn are present in the Sn_3O_4-Ti/b-TiO_2-3 curves, that in agreement with EDS mapping findings above. In the high-resolution spectra in Figure 4(b), the Ti 2p peaks are located at 459.1 and 464.8 eV in Ti/b-TiO_2, which are identical to previous work[46]. The blue-shift in Ti $2p_{3/2}$ and Ti $2p_{3/2}$ demonstrate the electron transfer from Sn_3O_4 to TiO_2. The asymmetric peaks of Sn 3d can be divided into two peaks, indicating the different chemical states of Sn (Sn^{2+} and Sn^{4+}) in heterostructure electrode Sn_3O_4-Ti/b-TiO_2-3 curves. After carefully fitting, the peaks of Sn $3d_{5/2}$ and Sn $3d_{3/2}$ in Figure 6(c) can be separated into two peaks (486.1 eV and 494.7 for Sn^{2+}) and (486.8 eV and 495.2 eV for Sn^{4+}), in sequence[47,48].

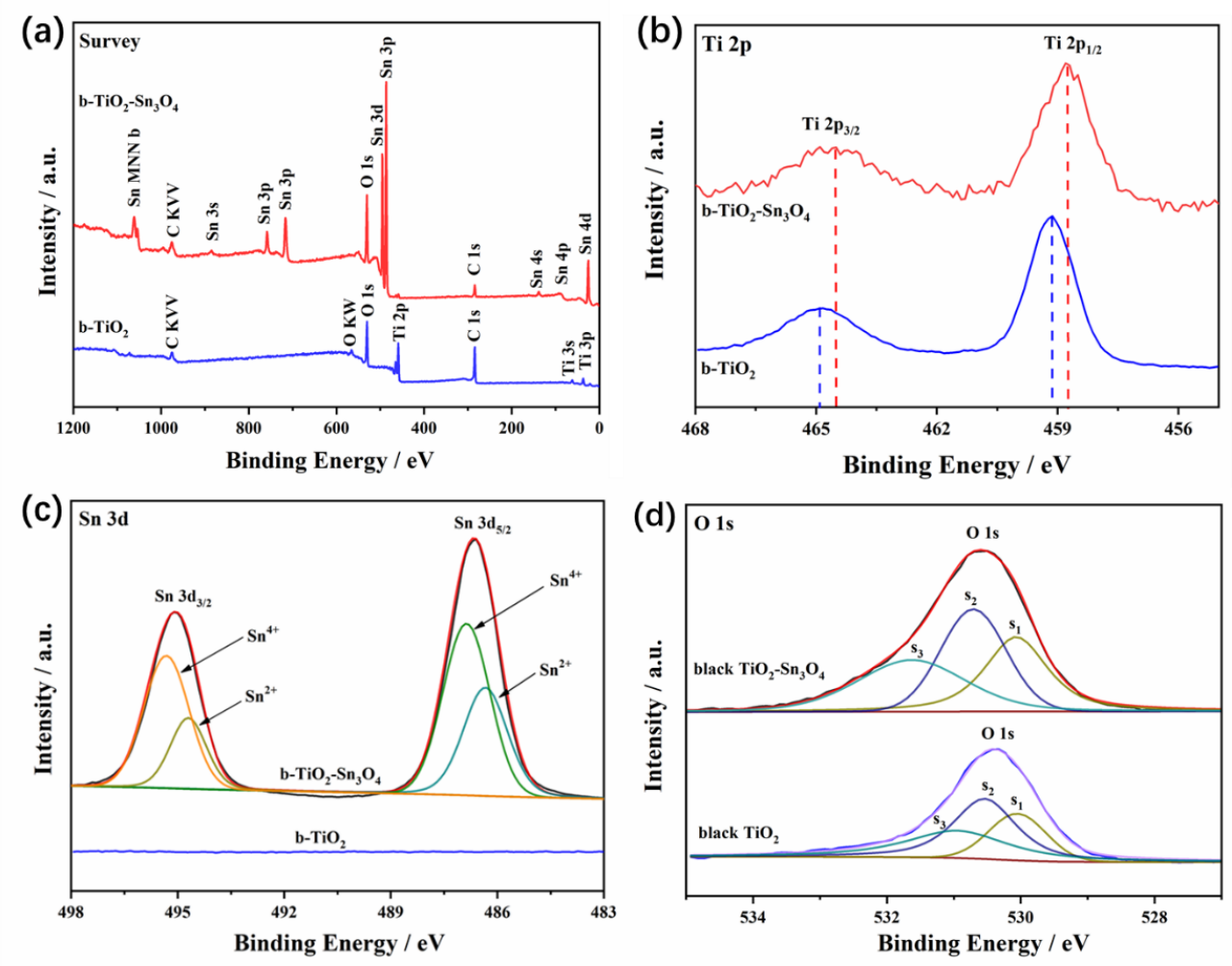

Figure 4. XPS spectra of Ti/b-TiO_2 and Sn_3O_4-Ti/b-TiO_2-3 electrodes. (a) Survey spectra, (b) Ti 2p spectra, (c) Sn 3d spectra and (d) O 1s spectra.

O1s spectrum is shown in Figure 6(d), the lower binding energy at 529.8 ~ 530.6 eV due to lattice oxygen (mostly O^{2-} ions). While the higher binding energy regions at 531.4–532.3 eV (s2 and s3 peaks) probably come from adsorbed or chemisorbed OH^- groups and H_2O on the oxide surface[49]. The hydroxyl groups on the electrode surface can be trapped with the holes induced by light and electricity to form hydroxyl radicals (•OH), which in turns inhibit electron-hole recombination and improve the photocatalytic efficiency[50]. And the higher intensity of s2 and s3 peaks in Sn_3O_4-Ti/b-TiO_2-3 indicate that the photocatalyst activity of the modified heterostructure hybrid electrode may have potentially higher photocatalytic activity.

3.2. Photoelectrochemical characteristics

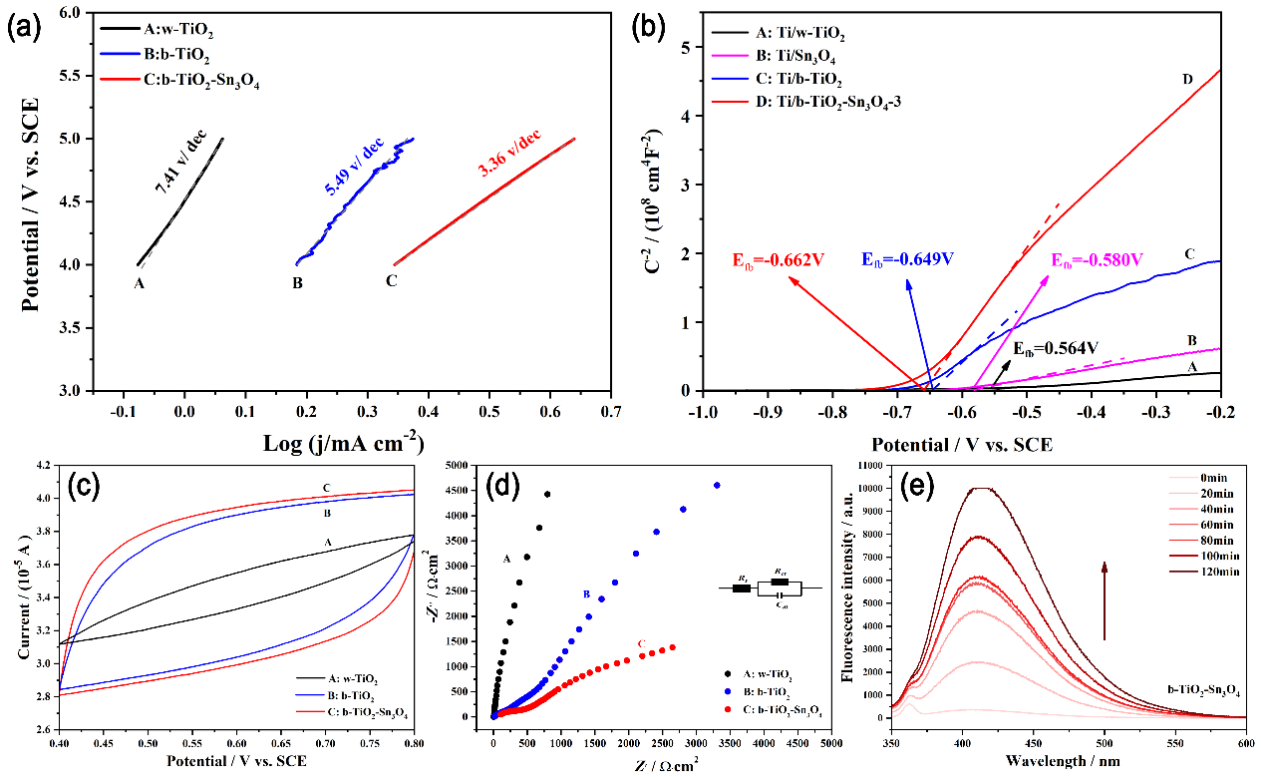

Figure 5. (a) Tafel Curve, (b) Mott-Schottky curve, (c) cyclic voltammetry curve and (d) electrochemical impedance spectroscopy (EIS) of Ti/w-TiO_2, Ti/b-TiO_2 and Sn_3O_4-Ti/b-TiO2 electrodes, the insert is equivalent circuit. (e) the photoluminescence spectrum of Sn_3O_4-Ti/b-TiO2-3 electrode.

The steady-state polarization test of Ti/w-TiO_2, Ti/b-TiO_2 and Sn_3O_4-Ti/b-TiO_2-3 electrodes were carried out to evaluate their oxidation capabilities and converted into Tafel curves with fitting to Tafel equation in Figure 5(a) [46]. The Tafel slope mainly reflects the reaction kinetics during electrocatalysis, and smaller Tafel slope values also indicate faster charge transfer speed[51]. As shown in Figure 5(a), the Sn_3O_4-Ti/b-TiO_2-3 has a smaller Tafel slope than the Ti/b-TiO_2. So, it can be inferred that the introduction of Sn_3O_4 increased the carrier transport efficiency of TiO_2, which would enhance its PEC performance. Figure 5(b) illustrates the Mott-Schottky (M-S) plots of Ti/w-TiO_2, Ti/b-TiO_2 and

Sn_3O_4-Ti/b-TiO_2-3 electrodes. All the M-S curves present a positive slope, indicating that they are n-type semiconductors. The flat band potentials (E_{fb}) of Ti/w-TiO_2, Ti/b-TiO_2, Ti-Sn_3O_4 and Sn_3O_4-Ti/b-TiO_2-3 composite electrodes are -0.56 eV, -0.65 eV, -0.58 eV and -0.66 eV *vs* SCE. The most negative E_{fb} of Sn_3O_4-Ti/b-TiO_2-3 shows the lowest resistance, the highest carrier separation rate and carrier density in these electrodes. The cyclic voltammetry (CV) curves of Ti/w-TiO_2, Ti/b-TiO_2 and Sn_3O_4-Ti/b-TiO_2-3 for all electrodes at a fixed current density are presented in Figure 5(c). The voltametric charge is commonly used to estimate the effective area of the electrode material and the number of active sites, which can be predicted by the area within the cyclic voltametric curve[52]. The voltametric curve area of the Ti/b-TiO_2 composite electrode is larger than the Ti/w-TiO_2 electrode, suggesting that the hydrogenation treatment can effectively increase the surface active sites of the electrode. As expected, the introduction of Sn_3O_4 can further increase the active sites on the electrode surface, and the Sn_3O_4-Ti/b-TiO_2-3 electrode exhibits the largest confinement area, which points to its excellent catalytic performance. Electrochemical impedance spectroscopy (EIS) was conducted to investigate the charge transfer characteristics of Ti/w-TiO_2, Ti/b-TiO_2 and Sn_3O_4-Ti/b-TiO_2 composite electrodes. Figure 5(d) displayed the EIS of Ti/w-TiO_2, Ti/b-TiO_2 and Sn_3O_4-Ti/b-TiO_2-3 experimental data. Basically, lower Rct values with smaller arc radius are corresponding to lower charge transfer resistance and fast interfacial carrier transfer procedures [53]. The results are consistent with the M-S analyses, Sn_3O_4-Ti/b-TiO_2-3 presented the smallest Rct value.

The concentration of •OH generated during the photoelectrochemical reaction was indicated by measuring the photoluminescence (PL) spectroscopy of a 1.64 mmol/L benzoic acid solution under continuous electrolysis in simulated sunlight conditions. Figure 5(e) represents the PL spectra of the electrolyte at different PEC times after employing Sn_3O_4-Ti/b-TiO_2-3 electrodes. With the increasing electrolysis time, the fluorescence intensity of the Sn_3O_4-Ti/b-TiO_2-3 electrode system remains consistently, which indicates more •OH could be produced at the Sn_3O_4-Ti/b-TiO_2-3 electrode. As the ability of the electrode to generate hydroxyl (•OH) is proportional to its PEC performance, the Sn_3O_4 modified Ti/b-TiO_2 electrode would possess higher PEC activity. According to the structural characterization and electrochemical performance tests, it can be revealed that Sn_3O_4-Ti/b-TiO_2-3 has a homogeneous heterogeneous structure and excellent photoelectric activity, which provides great promise for its applications in the field of PEC.

3.3. Characterization and mechanism investigation of PEC toward dye degradation with heterojunction electrode

The PEC degradation performance was evaluated through the decolorization rates of RBB KN-R aqueous solution with Ti/w-TiO_2, Ti/b-TiO_2 and Sn_3O_4-Ti/b-TiO_2 electrodes. As illustrated in Figure 6(a), the removal rate of RRB KN-R was improved from ~20% to ~70% with hydrogenation treatment of the Ti/w-TiO_2 electrode. Moreover, the addition of Sn_3O_4 could further enhance the degradation efficiency, and the decolorization rate of RRB KN-R with the Sn_3O_4-modified electrode reached above 79%. Among them, Sn_3O_4-Ti/b-TiO_2-3 presents the best degrade performance with the highest degradation rate of 85% for RRB KN-R. The synergistic effect of photocatalyst and electrocatalyst for the degradation of RRB KN-R under photocatalysis (PC), electrocatalysis (EC) and PEC processes with

Ti/b-TiO_2 and Sn_3O_4-Ti/b-TiO_2-3 electrodes was investigated and summarized in Figure 6(b). It is noteworthy the degradation efficiency of RRB KN-R with the both electrodes under PEC conditions was higher than the sum of EC and PC. The catalytic performances of the semiconductor materials for RRB KN-R degradation are listed in Table 1. With the consideration of factors, such as light source intensity and substrate concentration, the Sn_3O_4 decorated black TiO_2 electrode presents a good decolorization ability. For further exploring the application potential of Sn_3O_4-Ti/b-TiO_2-3 electrodes in actual industrial production, sodium chloride and sodium dodecylsulfonate were added into RRB KN-R solution as auxiliary salt and emulsifier to simulate the dye wastewater[54]. Figure 6(c) compared the decolorization performances of Ti/w-TiO_2, Ti/b-TiO_2 and Sn_3O_4-Ti/b-TiO_2 electrodes in RRB KN-R solution/simulated wastewater. The synthesized electrodes remained stable PEC behavior in both environments, where the slight decrease in decolorization rate could be attributed to the blocking effect of chloride ions. [55] Five cycles of degradation experiments on the Sn_3O_4-Ti/b-TiO_2-3 electrode were conducted to study its stability and the results are shown in Figure 6(d). The Sn_3O_4-Ti/b-TiO_2-3 electrode demonstrates only an 8% reduction in the degradation performance, indicating a promising prospect for applying in the field of dye degradation and wastewater treatment.

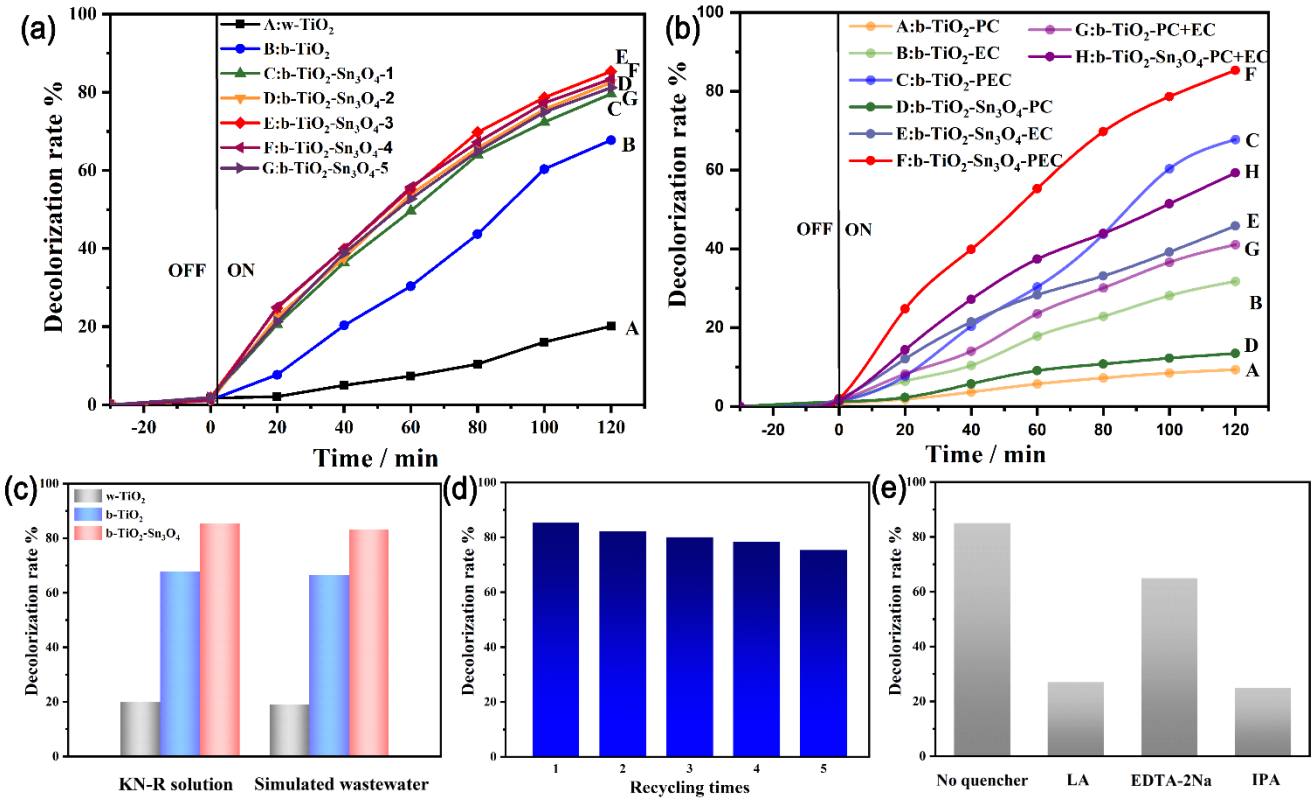

Figure 6. (a) Degradation rate of RRB KN-R over Ti/w-TiO_2, Ti/b-TiO_2 and Sn_3O_4 modified electrodes. (b) The RRB KN-R removal performance of Ti /b-TiO_2 and Sn_3O_4-Ti/b-TiO_2-3 electrode in different reaction conditions (PE, EC and PEC). (c) Removal efficiency of Ti/w-TiO_2, Ti/b-TiO_2 and Sn_3O_4-Ti/b-TiO_2 toward different kinds of water. (d) Five times recycling experiments of Ti/b -TiO_2-Sn_3O_4-3 electrode. (e) Evaluation of active species during decolorization of dyeing wastewater using Sn_3O_4-Ti/b-TiO_2-3 as photoanode.

Table 1. The comparison of catalytic performance of semiconductor materials through the degradation of RRB KN-R in 2h.

Material features	Degradation method	Light source	Concentration of dye (mg/L)	Decolorization rate (%)	Reference
Sn_3O_4-Ti/b-TiO_2	PEC	10W ultraviolet lamp	60	85	This work
Ti/Co_3O_4-Sn_3O_4	PEC	10W ultraviolet lamp	60	87.5	52
F-doped Ti/Co_3O_4	PEC	10W ultraviolet lamp	60	84	56
BN modified Ti/PbO_2	PEC	10W ultraviolet lamp	60	94.3	57
N-doped TiO_2	PC	125W high-pressure mercury lamp	60	98	58
Sn-SnO_2/C	PC	500W xenon lamp	20	40	59
Cu-Cu_2O-CuO/active carbon	PC	500W xenon lamp	20	76	60
$(BiO)_2CO_3$/Bi_2S_3	PC	300W xenon lamp	30	97	61
carbon black-modified Ti/F-PbO_2	PEC	175W xenon lamp	60	67	62
Black TiO_2 nanotube arrays	PEC	175W xenon lamp	60	75	63

We utilized isopropanol (IPA), EDTA-2Na^+ and L-ascorbic acid (LA) to quench •OH, h^+ and •O_2^- for detecting the active free radicals generated *via* Sn_3O_4-Ti/b-TiO_2-3 electrode in the PEC degradation procedure (Figure 6(e)) [46]. As summarized in Figure 6 (e), the degradation rate of RRB KN-R with Sn_3O_4-Ti/b-TiO_2-3 electrode was significantly inhibited to 26.9% and 24.7% after the addition of LA and IPA, which revealed that •OH and •O_2^- are the dominant reactive radicals in the PEC process. Meanwhile, the EDTA-2Na^+ incorporation also depressed the PEC activity, which verified the presence of cavities in the PEC process, but its effects were less than the former ones.

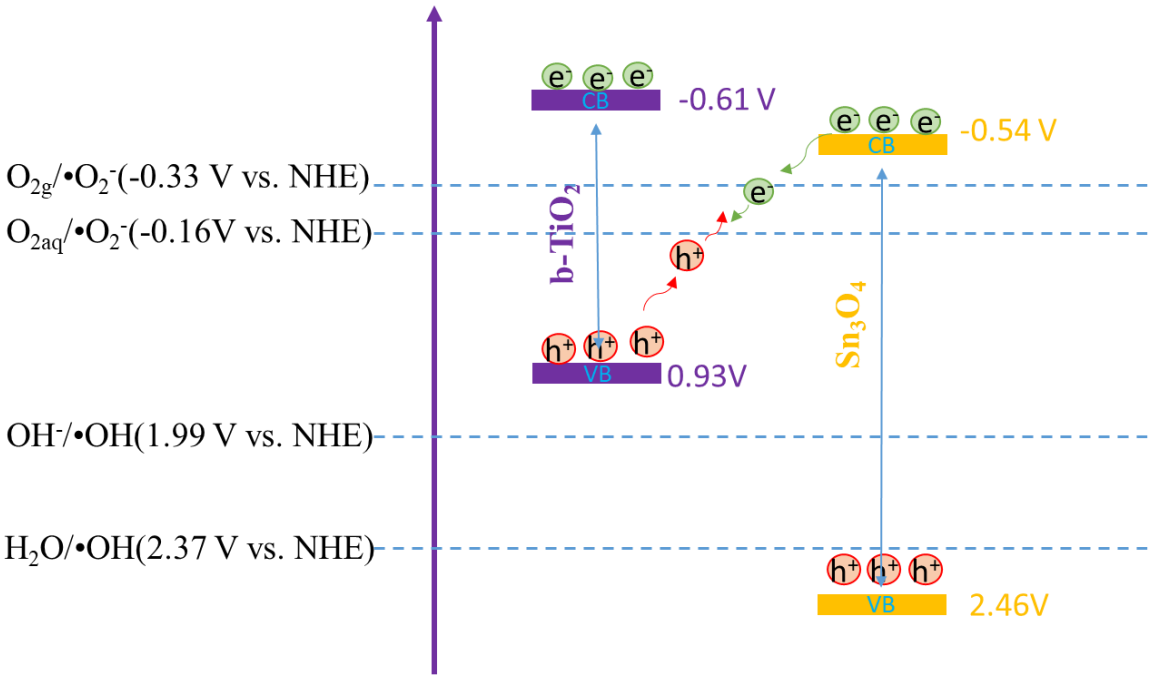

Scheme 2 Schematic diagram of the photoelectrocatalytic mechanism of the Sn_3O_4-Ti/b-TiO_2 electrode.

To further clarify the electron transport process in the Sn_3O_4-Ti/b-TiO_2 heterostructure, proposed band structures of b-TiO_2 and Sn_3O_4 electrode are illustrated in Scheme 2. With a positive slope in the Mott-Schottky plot (Figure 5b), b-TiO_2 and b-TiO_2-Sn_3O_4-3 presented the behavior of n-type semiconductor. Generally speaking, the Fermi level is equal to the flat band potential in n-type semiconductor, while the bottom of the conduction band (CB) is ~0.2 eV negative than Fermi level[64,65]. Therefore, the potential CB of b-TiO_2 and Sn_3O_4 can be estimated to be -0.61 and -0.54 V vs. NHE. And the forbidden bandwidth of b-TiO_2 and Sn_3O_4 are reported at 1.54 eV and 3.0 eV[26,52,66,67]. Based on their energy band structures, the induced carrier migration paths can be assigned to the traditional type II or Z-scheme mechanisms. According to the fluorescence quenching investigation, the main reactive radicals are •OH and $•O_2^-$ (Figure 5d), and more •OH form during the PEC process (Figure 4). Hence, it is assumed that the favorable carrier transfer route of the b-TiO_2-Sn_3O_4 heterostructure can be ascribed to Z-scheme. The active species •OH and $•O_2^-$ can be generated in Z-scheme mechanisms from CB level of b-TiO_2 at -0.42 V (vs. NHE), which is higher than both E ($O_{2g}/•O_2^-$) at -0.33 V (vs. NHE) and E($O_{2aq}•O_2^-$) at -0.16 V (vs. NHE). And the VB of Sn_3O_4 (3.06 V vs. NHE) is sufficient enough to create the •OH in comparison with E (OH-/•OH: 1.99 V vs. NHE) and E ($H_2O/•OH$: 2.37 V vs. NHE). In a typical procedure, photogenerated electron and hole pairs appeared in the conduction band (CB) and valence band (VB) of both semiconductors b-TiO_2 and Sn_3O_4 under light irradiation. Subsequently, the electrons in the CB flew to the counter electrode through the external circuit at a bias potential above the flat band potential. The hole (h^+) in the VB could oxidize H_2O molecules and OH^- ions adsorbed on the electrode surface to create hydroxyl radicals (•OH) or directly oxidize the dye molecules. And O_2 existed in air and solution could generation reactive oxygen species

($\bullet O_2^-$) with electrons. The •OH and $\bullet O_2^-$ are highly oxidizing active species that are capable enough to oxidize organic dye molecules.

4. CONCLUSION

To summarize, a novel photoelectrode combined with black TiO_2 and Sn_3O_4 nanosheets was fabricated through a two-step hydrothermal process. The hydrogenation of white TiO_2 to black TiO_2 enabled the electrode with better light absorption performance and increased the quantity of photogenerated electron-hole pairs produced by the composite electrode. The black TiO_2 was further modified with a secondary hydrothermal method, and the size of the Sn_3O_4 nanosheets could be adjusted *via* changing the concentration of the hydrothermal solution, resulting in a tight adhesion of the Sn_3O_4 nanosheets to black TiO_2 nanoflowers. The introduction of Sn_3O_4 on the surface of black TiO_2 coating could negatively shift its flat band potential and generate more hydroxyl radicals, leading to the enhancement of the electron hole transfer rate and electrochemically active area. The composite electrodes showed a 3-fold increase in RBB KN-R removal rate compared to the original white TiO_2 one. Sn_3O_4-Ti/b-TiO_2-3 was the most outstanding one demonstrating the degradation rate of 85 % and long-term stability for the degradation of reactive brilliant blue KN-R in 0.1 mol/L Na_2SO_4 solutions. Therefore, the photoelectrodes constructed with the black TiO_2 and Sn_3O_4 heterostructure hold great potential for practical applications in the decomposition of organic pollutants. This work offers a new strategy for the construction of layered heterojunction photoanode materials with high PEC efficiency.

CONFLICTS OF INTEREST
There are no conflicts of interest to declare.

ACKNOWLEDGMENTS
This work was supported by the National Natural Science Foundation of China (21875026, 21878031), the Liaoning Revitalization Talents Program (XLYC1802124). The Project is also sponsored by Liaoning BaiQianWan Talents Program, the scientific research fund of the educational department of Liaoning province (J2019013). This work was also supported by Joint Research Fund Liaoning-Shenyang National Laboratory for Materials Science (Project number: 2019JH3/30100034; Contract number: 2019010278-JH3/301).

References

1. B. K. Körbahti, A. Tanyolaç, *J. Hazard. Mater*., 151 (2008) 422.
2. S. Lin, C. Peng, *Water Res*., 28 (1994) 277.
3. E. G. Solozhenko, N. M. Soboleva, V. V. Goncharuk, *Water Res*., 29 (1995) 2206.
4. V. M. Correia, T. Stephenson, S. J. Judd, *Environ. Technol. Rev*., 15 (1994) 917.
5. J. Paprowicz, S. Slodczyk, *Environ. Sci. Technol. Lett*., 9 (1988) 271.
6. S. -H. Lim, N. Ç. Gürsoy, P. Hauser, D. Hinks, *Color. Technol*., 120 (2004) 114.
7. C. Hu, Y. Wang, *Chemosphere*, 39 (1999) 2107.
8. N. Mohan, N. Balasubramanian, C. A. Basha, *J. Hazard. Mater*., 147 (2007) 644.

9. S. Chakrabarti, B. K. Dutta, *J. Hazard. Mater*., 112 (2004) 269.
10. K. Esquivel, L. G. Arriaga, F. J. Rodríguez, L. Martínez, L. A. Godínez, *Water Res.*, 43 (2009) 3593.
11. F. M. M. Paschoal, M. A. Anderson, M. V. B. Zanoni, *Desalination*, 249 (2009) 1350.
12. J. Luo, M. Hepel, *Electrochim. Acta*, 46 (2001) 2913.
13. P. Li, G. Zhao, M. Li, T. Caoa, X. Cui, D. Li, *Appl. Catal. B*, 111-112 (2012) 578.
14. S. Garcia-Segura, E. Brillas, *J. Photochem. Photobiol*. C, 31 (2017) 1.
15. G. G. Bessegato, T. T. Guaraldo, J. F. de Brito, M. F. Brugnera, M. V. B. Zanoni, *J. Electroanal. Chem.,* 6 (2015) 415.
16. D. Liu, R. Tian, J. Wang, E. Nie, X. Piao, X. Lia, Z. Sun, *Chemosphere*, 185 (2017) 574.
17. L. Xu, Q. Jiang, Z. Xiao, X. Li, J. Huo, S. Wang, L. Dai, *Angew. Chem. Int. Ed*., 128 (2016) 5356.
18. G. Zhao, X. Cui, M. Liu, P. Li, Y. Zhang, T. Cao, H. Li, Y. Lei, L. Liu, D. Li, *Environ. Sci. Technol.*, 4227 (2009) 1480.
19. Y. Lee, J. Suntivich, K. J. May, E. E. Perry, Y. Shao-Horn, *J. Phys. Chem. Lett*., 29047 (2012) 399.
20. J. Liu, Y. Zheng, Y. Jiao, Z. Wang, Z. Lu, A. Vasileff, S. -Z. Qiao, *Small*, 14 (2018) 16.
21. J. Lim, D. Park, S. S. Jeon, C. -W. Roh, J. Choi, D. Yoon, M. Park, H. Jung, H. Lee, *Adv. Funct. Mater.,* 28 (2018) 4.
22. J. Lyu, H. Han, Q. Wu, H. Ma, C. Ma, Xi. Dong, Y. Fu, *J Solid State Electrochem*., 23(2019) 847.
23. J. Cai, M. Zhou, Y. Pan, X. Du, X. Lu, *Appl. Catal*. B, 257 (2019) 19.
24. Y. Liu, Y. Jiao, Z. Zhang, F. Qu, A. Umar, X. Wu, *ACS Appl. Mater. Inter*., 5550 (2014) 2174.
25. G. Zhao, Y. Zhang, Y. lei, B. Lv, J. Gao, Y. Zhang, D. Li, *Environ. Sci. Technol*., 2940 (2010) 1754.
26. J. Lyu, G. Sun, L. Zhu, H. Ma, C. Ma, X. Dong, Y. Fu, *J Solid State Electrochem*., 24 (2020) 375.
27. T. Song, R. Li, N. Li, Y. Gao, *Sci Adv. Mater*., 11 (2019) 258.
28. G. Chen, J. Wang, C. Wu, C. Li, H. Jiang, X. Wang, *Langmuir,* 1348 (2018) 12393.
29. A. Fujishima, K. Honda, *Nature*, 238 (1972) 37.
30. K. Vinodgopal, D. E. Wynkoop, P. V. Kamat, *Environ. Sci. Technol*., 3507 (1996) 1660.
31. M. D. Hernández-Alonso, F. Fresno, S. Suárez, J. M. Coronado, *Sol. Energy*, 2 (2019) 1231.
32. H. Dong, G. Zeng, L. Tang, C. Fan, C. Zhang, X. He, Y. He, *Water Res*., 79 (2015) 128.
33. X. Chen, L. Liu, P. Y. Yu, S. S. Mao, *Science*, 331 (2011) 746.
34. Y. Liu, L. Tian, X. Tan, X. Li. X. Chen, *Sci. Bull*., 62 (2017) 431.
35. J. Kim, K. Zhu, Y. Yan, C. L. Perkins, A, J. Frank, *Nano Lett*., 7563 (2010) 4099.
36. M. Chandra, K. Bhunia, D. Pradhan, *Inorg. Chem*., 2432 (2018) 4524.
37. D. Rajamanickam, P. Dhatshanamurthi, M. Shanthi, *Mater. Res. Bull*., 61 (2015) 439.
38. H. He, J. Lin, W. Fu, X. Wang, H. Wang, Q. Zeng, Q. Gu, Y. Li, C. Yan, B. K. Tay, C. Xue, X. Hu, S. T. Pantelides, W. Zhou, Z. Liu, *Adv. Funct. Mater*., 6 (2016) 464.
39. J. Papp, S. Soled, K. Dwight, A. Wold, *Chem. Mater*., 3434 (1994) 496.
40. W. Zhou, H. Liu, J. Wang, D. Liu, G. Du, J. Cui, *ACS Appl. Mater. Inter*., 7194 (2010) 2385.
41. A. Huda, P. H. Suman, L. D. M. Torquato, B. F. Silva, C. T. Handoko, F. Gulo, M. V. B. Zanoni, M. O. Orlandi, *J. Photochem. Photobiol*. A, 376 (2019) 196.
42. H. J. Queisser, E. E. Hallller, *Science*, 281 (1998) 945.
43. M. Manikandan, T. Tanabe, P. Li, S. Ueda, G. V. Ramesh, R. Kodiyath, J. Wang, T. Hara, A. Dakshanamoorthy, S. Ishihara, K. Ariga, J. Ye, N. Umezawa, H. Abe, *ACS Appl. Mater. Inter*., 4832 (2014) 3790.
44. X. Yu, L. Wang, J. Zhang, W. Guo, Z. Zhao, Y. Qin, X. Mou, A. Li, H. Liu, *J. Mater. Chem*. A, 3 (2015) 19129.
45. X. Yu, Z. Zhao, D. Sun, N. Ren, J. Yu, R. Yang, H. Liu, *Appl. Catal*. B, 227 (2018) 470.
46. J. Lyu, G. Sun, L. Zhu, H. Ma, C. Ma, X. Dong, Y. Fu, *J Solid State Electrochem*., 24 (2020) 375.
47. W. Xia, H. Wang, X. Zeng, J. Han, J. Zhu, M. Zhou, S. Wu, *CrystEngComm*, 16 (2014) 6841.
48. X. Ma, J. Shen, D. Hu, L. Sun, Y. Chen, M. Liu, C. Li, S. Ruan, *J. Alloys Compd*., 726 (2017) 1092.

49. G. Chen, S. Ji, Y. Sang, S. Chang, Y. Wang, P. Hao, J. Claverie, H. Liu, G. Yu, *Nanoscale*, 7 (2015) 3117.
50. L. Yan, Y. Cheng, S. Yuan, X. Yan, X. Hu, K. Oh, *Res. Chem. Intermed*., 39 (2013) 1763.
51. X. Chen, D. Wang, Z. Wang, P. Zhou, Z. Wu, F. Jiang, *Chem. Commun*., 50 (2014) 11683.
52. M. Li, W. Li, J. Lyu, M. A. Moussa, X. Liu, Y. Fu, H. Ma, *Chem. Eng. J.*, 423 (2021) 130252.
53. Y. Di, C. Ma, Y. Fu, X. Dong, X. Liu, H. Ma, *ACS Appl. Mater. Interfaces* 518 (2021) 8405.
54. G. Zhang, J. Yang, Z. Guo, J. Sun, *Method for improving dyeing uniformity of KN-R reactive dye.* China unveiled patent number: CN112522970A
55. P. Wang, S. Yang, L. Shan, R. Niu, X. Shao, *J. Environ. Sci.* 23 (2011) 1799.
56. H. Ma, X. Wang, Y. Fu, Y. Zhang, C. Ma, X. Dong, Z. Yu, *J. Solid. State. Electrochem.* 23 (2019) 1767.
57. H. Han, J. Lyu, L. Zhu, G. Wang, C. Ma, H. Ma, *J. Alloys. Compd.* 828 (2020) 154049.
58. S. Hua, A. Wang, X. Li, H.Löwec, *J. Phys. Chem. Solids.* 71 (2010) 156.
59. H. Ma, K. Teng, Y. Fu, Y. Song, Y. Wang, X. Dong, *Energy. Environ. Sci.* 4 (2011) 3067.
60. H. Ma, Y. Liu, Y. Fu, C. Yu, X. Dong, X. Zhang, X. Zhang, W. Xue, *Aust. J. Chem.* 67 (2013) 749.
61. M. Zhao, Y. Fu, H. Ma, C. Ma, X. Dong, X. Zhang, *Mater. Des.* 93 (2016) 1.
62. K. Zhou, Y. Tian, H. Ma, C. Ma, Y. Fu, X. Dong, X. Zhang, *J. Solid. State. Electrochem.* 22 (2018) 131.
63. L. Zhu, H. Ma, H. Han, Y. Fu, C. Ma, Z. Yu, X. Dong, *RSC Adv.* 8 (2018) 18992.
64. H. Yi, M. Yan, D. Huang, G. Zeng, C. Lai, M. Li, X. Huo, L. Qin, S. Liu, X. Liu, B. Li, H. Wang, M. Shen, Y. Fu, X. Guo, *Appl. Catal. B*, 250 (2019) 52.
65. J. Lyu, X. Liu, Y. Chen, H. Li, R. Li, X. Dong, H. Lee, H. Ma, *J. Phys. Chem. C*, 480 (2020) 11525.
66. X. Chein, L. Liu, P. Y. Yu, S. S. Mao, *Science*, 331 (2011) 746.
67. A. Naldoni, M. Altomare, G. Zoppellaro, N. Liu, Š. Kment, R. Zbořil, P. Schmuki, *ACS Catal.*, 14658 (2019) 345.